Digest Journal of Nanomaterials and Biostructures

Dig. J. Nanomater. Bios. **2026**; 21(3): 52584
https://doi.org/10.31083/DJNB52584

Original Research

Effects of Zn and Ag (Co)Doping on the Structural, Optical, and Antibacterial Properties of CuO Nanoparticles

Abbas Fouzia[1,*], Attaf Sonia[2], Ouassila Benzoui[3], Ouidad Abedlaziz[4], Fakher Hana[1], Zaibet Asma[1]

[1]Department of Physics, Laboratory of Microstructure and Defect in Materials, University Constantine 1, 25000 Constantine, Algeria
[2]Department of Physics, Laboratory of Ceramic, University Constantine 1, 25000 Constantine, Algeria
[3]Department of Physics, Laboratory of Thin Films and Interface, University Constantine 1, 25000 Constantine, Algeria
[4]Department of Microbiology, Laboratory of Applied Biochimie, University Constantine 1, 25000 Constantine, Algeria
*Correspondence: fouzia.abbas@umc.edu.dz (Abbas Fouzia)
Academic Editor: Karol Kyzioł
Submitted: 3 April 2026 Revised: 10 June 2026 Accepted: 17 June 2026 Published: 16 September 2026

Abstract

Background: Copper oxide (CuO) nanoparticles exhibit high structural, optical, and antibacterial properties; co-doping with Zn and Ag can further modify these properties but comparative studies of single and co-doped CuO synthesized by sol-gel are limited. This study evaluates the effects of Zn (5 at %), Ag (5 at %), and Zn + Ag (5 at % each) doping on the structure, optical, morphology, and antibacterial activity of CuO nanoparticles. **Methods:** Pure CuO nanoparticles (NPs) and those doped with Zn (5 at %), Ag (5 at %), and Zn + Ag (5 at % each) were prepared using a sol-gel method and characterized in terms of structural, optical, and antibacterial properties. **Results:** All samples exhibited the monoclinic tenorite structure. Doping reduced crystallite size and increased defect (e.g., dislocation) density, microstrain, and unit cell volume. The NPs exhibited a homogeneous distribution and featured dopant-dependent morphologies and aggregation extents. Doping increased the absorbance of CuO in the visible region, with the band gaps of pure and Zn/Ag-codoped NPs determined as 1.77 and 1.71 eV, respectively. All NPs inhibited the proliferation of *Escherichia coli* and *Staphylococcus aureus* (model Gram-negative and Gram-positive bacteria, respectively). The strongest effect was observed for codoped CuO, which inhibited *E. coli* more than it did *S. aureus*. **Conclusions:** Thus, Zn/Ag-codoped CuO NPs hold promise for different applications, particularly those requiring antibacterial properties.

Keywords: CuO nanoparticles; Zn/Ag doping; sol-gel method; structural properties; optical properties; antibacterial efficacy

1. Introduction

The small size and large surface area of nanoparticles (NPs) endow them with properties markedly different from those of bulk materials, enabling diverse applications such as the diagnosis and treatment of diseases previously considered intractable [1,2,3]. Other advantages of NPs include high stability, simple synthesis, and precisely controllable properties such as size, shape, and porosity [4]. CuO NPs find diverse applications, including gas sensing, solar energy harvesting, photocatalysis, and microbe eradication [5,6,7,8], outperform their bulk counterparts in terms of performance, stability, and sensitivity as antimicrobial agents [9], and are available in diverse shapes, including nanotubes, nanorods, nanowires, and nanospheres [10].

CuO NPs demonstrate high efficacy against resistant strains of pathogenic bacteria and possess low cytotoxicity, thus holding promise for critical applications such as healthcare and water treatment [11]. This remarkable antibacterial activity depends on multiple factors and is attributed to the strong interactions between bacterial cell membranes and CuO NPs enabled by the large surface area and small size of the latter [12]. CuO NPs are typically prepared by ball milling and hydrothermal treatment [13,14]. The sol-gel method offers the advantages of good homogeneity, easy composition adjustment, low reaction temperature, and the possibility of accessing different morphologies [15]. Cu has three oxidation states (I–III) and is therefore suitable for both electron and hole doping [16]. Moreover, CuO is widely used in photocatalysis, electronics, and biomedicine [17,18].

The simultaneous doping of semiconductor oxides such as CuO by two transition elements can impart properties inaccessible via single-element doping [19]. The elements used to (co)dope CuO NPs include Ni [20], Mg [21], Co [22], Ag [23], Fe/Co [24], Ag/Ni [25], and Ag/Zn [26]. CuO NPs exert antimicrobial effects through the release of Cu^{2+} [27], while ZnO exerts such effects by promoting the generation of reactive oxygen species (ROS) [28,29]. The doping of CuO with Zn^{2+} is feasible because the ionic radius of Cu^{2+} (0.72 Å) is similar to that of Zn^{2+} (0.74 Å) and creates defects that may result in enhanced antibacterial activity [30]. Ag-doped CuO NPs hold particular promise because of the nature of Ag^{+} ions, and exhibit antibacterial properties well suited for water treatment and cosmetic applications [25,31]. Azam et al. [32] explored the activity of CuO NPs against Gram-positive and Gram-negative

bacteria. Dadi et al. [33] reported that ZnO and CuO NPs deposited by diffusion methods show high activity against Gram-negative (e.g., *Escherichia coli*) and Gram-positive (e.g., *Staphylococcus aureus*) bacteria. Several works examined transition metal (e.g., Zn, Ag, and Zn/Ag)-doped CuO NPs [34,35,36].

Herein, we explore the structural, optical, morphological, and antibacterial properties of pristine and Ag-doped, Zn-doped, and Ag/Zn-codoped CuO NPs prepared using a sol-gel method, revealing that Zn/Ag-codoped CuO NPs exhibit remarkable activity against *E. coli* (ATCC-25922) and *S. aureus* (ATCC-43300).

2. Materials and Methods

2.1 Materials

$Cu(NO_3)_2 \cdot 3H_2O$ (≥99.0%), citric acid (≥99.0%), $Zn(CH_3COO)_2 \cdot 2H_2O$ (≥98–99%), $AgNO_3$ (≥99.0%), and absolute ethanol (≥99.5%) were supplied by Sigma-Aldrich. Distilled water was obtained from a standard laboratory water purification system. All chemicals were used as received without further purification.

2.2 Equipment

CuO NPs were characterized using X-ray diffraction (XRD, X'Pert MPD, Philips Analytical, Almelo, The Netherlands), Fourier transform infrared (FTIR) spectroscopy (FTIR, FT/IR-4700, JASCO International Co., Ltd., Hachioji, Tokyo, Japan), ultraviolet–visible (UV–vis) spectroscopy (UV–Vis, V-630, JASCO International Co., Ltd., Hachioji, Tokyo, Japan), and field-emission scanning electron microscopy (FE-SEM, JSM-7600F, JEOL Ltd., Akishima, Tokyo, Japan).

2.3 Synthesis

$Cu(NO_3)_2 \cdot 3H_2O$ (5 g) was dispersed in ethanol–distilled water (25 mL) upon magnetic stirring. The dispersion was heated at 80 °C for 2 h upon stirring until a clear and homogeneous solution was obtained. Separately, citric acid (0.4 g) was dissolved in ethanol (25 mL) upon magnetic stirring, and the resulting solution was dropwise added to the copper nitrate solution upon stirring. The precipitate was collected, dried at 80 °C for 24 h, and crushed to a uniform consistency using a mortar and pestle. The resulting powder was heated at 500 °C for 4 h to afford pure CuO NPs. Doped CuO NPs were prepared using the same procedure but with the desired dopant ($Zn(CH_3COO)_2 \cdot 2H_2O$, $AgNO_3$, or both) codissolved with copper nitrate in the first step (Zn loading = Ag loading = 5 at %).

2.4 Antibacterial Activity Evaluation

Antibacterial activity was assessed using a diffusion assay [37]. Sterilized Mueller–Hinton agar was distributed into Petri dishes (4 mL per dish) and allowed to congeal. Sterile wells were created in the solidified agar using a sterile cork borer. Sterile wells measuring 6 mm in diameter and 4 mm in depth were used. The agar plates were allowed to cool for 10–15 min at room temperature (approximately 25 °C) before inoculation to prevent damage to bacteria and inoculated using two techniques. A diluted bacterial inoculum [10^7 colony-forming unit (CFU)/mL] was prepared and used to flood the entire agar surface, with excess liquid carefully removed. Alternatively, a sterilized cotton wipe was dipped in the inoculum and used to make streaks across the agar surface. After brief drying (4 min) to ensure bacterial adherence, each well was supplemented with CuO NPs (1 mg). All inoculated plates, including negative controls (no NPs) and positive controls (pristine and doped CuO NPs) were incubated at 37 °C for 24 h (Fig. 1).

Fig. 1. (A) Image illustrating the well diffusion assay used to evaluate antibacterial activity. (B) Images of *E. coli* (E) and *S. aureus* (S) growth on Mueller–Hinton agar.

3. Results and Discussion

3.1 XRD Analysis

The XRD patterns of pure CuO NPs (Fig. 2A) featured peaks at 2θ = 32.46°, 35.68°, 38.25°, 38.80°, 44.28°, 48.80°, 53.67°, 58.45°, 61.66°, 64.80°, 66.32°, 68.14°, 72.67°, 75.29°, and 77.89° corresponding to the (110), (002), (111), (200), (112), (–202), (020), (202), (–113), (022), (311), (220), (11–3), (22–2), and (004) planes, respectively, and agreed with the standard pattern of tenorite (ICSD No. 01-080-1268) [38]. No marked changes in the positions of peaks at 2θ = 35°–38° were observed upon Zn (Fig. 2B) and Ag (Fig. 2C) doping. However, the increase in peak intensity observed for these samples indicated their increased crystallinity. The slight peak shift to lower angles upon Zn and Ag incorporation was ascribed to the difference between the radii of dopant ions and Cu^{2+}. The pattern of Zn/Ag-codoped CuO NPs (Fig. 2D) exhibited additional peaks at 2θ = 27.77°, 34.31°, 46.44° and 54.68° corresponding to the (110), (200), (440) and (311) planes of the Ag–CuO phase, respectively, and matched those of monoclinic CuO (JCPDS No. 96-500-0076) and silver(III) oxide (JCPDS No. 00-040-0909). This pattern signified the formation of a secondary Ag–CuO phase alongside the dominant CuO phase [39]. The peaks at 2θ = 35° and 38°

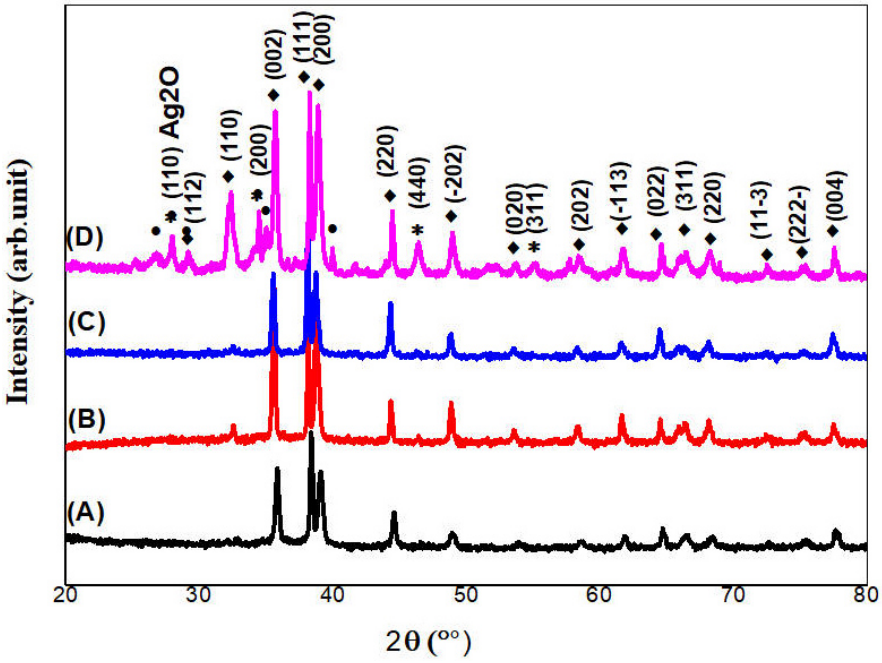

Fig. 2. XRD patterns of (A) pure, (B) Zn-doped, (C) Ag-doped, and (D) Zn/Ag-codoped CuO NPs. ♦: CuO NPs, *: Ag–CuO NPs.

Table 1. Selected structural parameters of pure and doped CuO NPs.

NPs	Average D (nm)	Average $\delta \times 10^{-4}$ (nm^{-2})	d_{110} (Å)	d_{002} (Å)	d_{200} (Å)	a (Å)	b (Å)	c (Å)	Average $\varepsilon \times 10^{-4}$	V (Å^3)
CuO	21.01	35.93	2.501	2.301	2.727	4.66	3.38	5.07	1.93	79.076
Zn-doped CuO	20.43	50.67	2.518	2.320	2.751	4.70	3.41	5.10	2.15	80.960
Ag-doped CuO	18.50	59.33	2.522	2.323	2.746	4.71	3.40	5.11	2.38	80.905
Zn/Ag-codoped CuO	15.92	52.78	2.512	2.313	2.760	4.69	3.43	5.09	2.39	81.050

CuO, copper oxide; NPs, nanoparticles.

commonly assigned to CuO might indicate an intermediate phase generated during Zn–CuO NP formation [40]. This finding necessitates the further investigation of the possibility of a minor Zn–CuO phase coexisting with the dominant CuO phase in the Zn-doped sample (Fig. 2B) even in the absence of pronounced peak position shifts.

The formation of Ag–CuO NPs in the codoped sample due to the dominance of Ag aligns with previous research [41,42] and suggests that Ag preferentially occupies Cu sites in the CuO lattice. However, Ag doping was reported to exert no notable influence on the crystal structure of CuO [43]. This discrepancy might be explained by considering ionic radii. Compared with the radius of Ag^+ (1.26 Å), that of Zn^{2+} (0.74 Å) is closer to that of Cu^{2+} (0.72 Å); hence, Zn^{2+} diffuses into the CuO lattice more efficiently than Ag^+ without markedly disrupting the host structure [44,45,46].

The average crystallite size (D) of NPs was calculated using the most intense XRD peaks according to the Scherrer equation [27]:

$$D = \frac{0.94\lambda}{\beta \cos\theta} \quad (1)$$

where λ = 1.546 Å is the X-ray wavelength, β (rad) is the full width at half-maximum of the employed peak, and θ is the peak angle. D and other structural parameters of pure and doped CuO NPs are listed in Table 1.

Average D followed the order of undoped CuO NPs (21.01 nm) > Zn-doped CuO NPs (20.43 nm) > Ag-doped CuO NPs (18.50 nm) > Zn/Ag-codoped CuO NPs (15.92 nm). This order reflects the effects of doping on crystal growth kinetics and the slight deterioration of the crystalline structure of CuO NPs [20]. Similar results have been described for Ag/Co-codoped CuO [25].

Dislocation density (δ), i.e., the number of dislocations per unit area of the crystal, was estimated as Eqn. 2 [47].

$$\delta = \frac{1}{D^2} \quad (2)$$

The average microstrain (ε) experienced by the crystal lattice was determined as Eqn. 3 [48].

$$\varepsilon = \frac{\beta \cos\theta}{4} \quad (3)$$

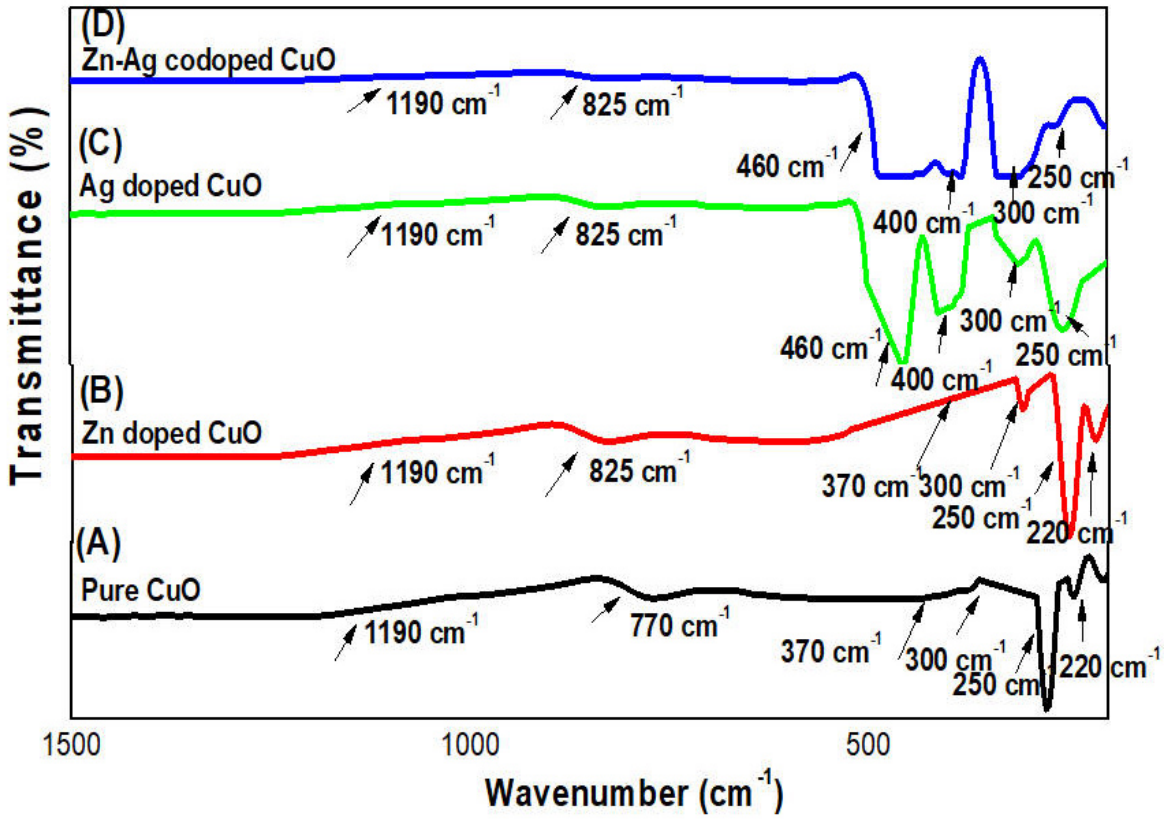

Fig. 3. FTIR spectra of pure and doped CuO NPs. (A) pure, (B), Zn-doped, (C) Ag-doped, and (D) Zn/Ag-codoped CuO NPs.

Interplanar spacings (d_{hkl}) and the unit cell volume (V) (Table 1) were determined as Eqns. 4,5 [27,46].

$$\frac{1}{d^2} = \frac{1}{\sin^2\beta}\left(\frac{h^2}{a^2} + \frac{k^2\sin^2\beta}{b^2} + \frac{l^2}{c^2} - \frac{2hl\cos(\beta)}{ac}\right) \quad (4)$$

$$V = abc\sin\beta \quad (5)$$

where a, b, and c are lattice parameters, h, k, and l are Miller indices, and β is the angle between the a and c axes.

Upon codoping, V increased from 79.076 to 81.050 Å^3 because of the size mismatch between Cu^{2+} and dopant ions and in addition to the anisotropy in the CuO crystal.

The decrease in D upon codoping was mirrored by an increase in δ and ε, which suggests an evolution of lattice imperfections, potentially due to alterations in NP microstructure and shape. The above findings align with previous observations [49,50].

3.2 FTIR Analysis

Fig. 3 presents the FTIR spectra of pure and doped CuO NPs. The most intense peaks in the spectrum of pure CuO NPs were observed between 220 and 770 cm^{-1} and ascribed to the stretching vibrations of Cu–O bonds in monoclinic CuO [51,52]. The bending vibrations of Cu–O, Zn–O, and Ag–O bonds were observed at around 460, 615 and 825 cm^{-1}, respectively [51,52]. The broad band at 1000–1500 cm^{-1} was ascribed to residual water vapor and atmospheric CO_2 [39].

The FTIR spectra of codoped CuO NPs featured additional strong peaks attributed to a secondary phase. This observation suggests that the substitution of Cu^{2+} with Zn^{2+} and Ag^{+} affected bond strength. The minor shifts in band arrangement upon codoping were attributed to the structural changes in the CuO lattice, supporting successful dopant incorporation. Overall, the results of FTIR analysis well align with those of XRD analysis.

3.3 Optical Properties

All samples exhibited absorbance in the visible and near-infrared (NIR) zones (Fig. 4) [53]. Pure CuO NPs showed the lowest overall absorbance, i.e., doping enhanced light-absorption ability. The absorption spectra displayed prominent peaks around 310 nm and an absorption border between 630–650 nm, which agrees with the bandgap transformation within CuO and indicates its crystalline structure [54]. Bhuvaneshwari and Gopalakrishnan [55] ascribed the peaks at 300–385 nm to exciton transitions in CuO. Wang et al. [56] ascribed the UV emission peak at 310 nm to the neighboring band-edge emission of CuO nanostructures arising from the recombination of electron–hole pairs in excitons. The red shift of absorption peaks upon codoping correlates with concomitant bandgap nar-

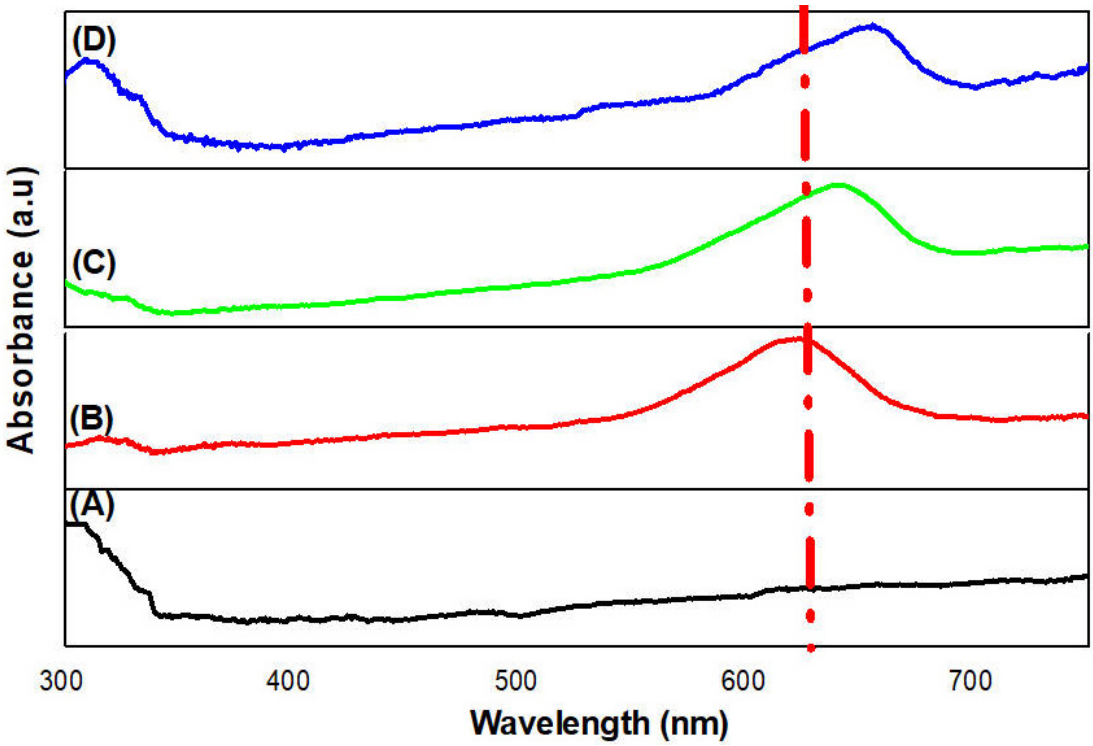

Fig. 4. UV–vis absorbance spectra of (A) pure, (B) Zn-doped, (C) Ag-doped, and (D) Zn/Ag-codoped CuO NPs. UV–vis, ultraviolet–visible.

rowing [57]. Simply put, codoped CuO absorbs light across a wider range (NIR to visible). Thus, both pure CuO and the co-doped sample exhibit absorption at approximately 300 nm, which corresponds to the UV region. However, the co-doped sample shows considerably higher absorption at wavelengths above 700 nm, indicating enhanced absorption in the NIR region. The above results show that codoping effectively extended the light absorption range of CuO NPs from the NIR to the visible region.

The bandgap of CuO NPs was determined using the Tauc equation [58]:

$$(\alpha h\nu)^n = B\,(h\nu – E_g) \tag{6}$$

where B is a material-specific constant, h is Planck's constant, υ is the photon frequency, E_g is the optical bandgap, n is an exponent determined by the nature of the electronic transition, and α is an absorption coefficient related to wavelength (λ) and extinction coefficient (k) as

$$\alpha = \frac{4\pi k}{\lambda} \tag{7}$$

Fig. 5 displays plots of $(\alpha h\upsilon)^2$ vs. $h\upsilon$ and the corresponding extrapolations used for bandgap determination. Band gaps were calculated by extrapolating the linear portion of the plots to the intercept with the $h\upsilon$ axis and decreased in the order of undoped CuO NPs (1.77 eV) > Zn-doped CuO NPs (1.75 eV) > Ag-doped CuO NPs (1.73 eV) > Zn/Ag-codoped CuO NPs (1.71 eV). This result is consistent with values of 1.5–2.1 eV reported elsewhere [56]. The bandgap decrease upon doping was due to the concomitant red shift of the absorption edge. Thus, codoped CuO NPs could absorb light of lower energy (longer wavelengths) than pure CuO, which was ascribed to the creation of additional energy states within the bandgap upon doping.

The incorporation of Zn and Ag can lead to lattice distortion and thus generate localized energy levels above the valence band. The energy required to excite the valence band to these newly formed levels is less than that required for direct excitation to the conduction band. Furthermore, the red shift can be attributed to the localization of charge carriers within the material structure and electron-phonon coupling arising from interactions at defect sites and interfaces. These combined effects facilitate the absorption of smaller-energy photons, leading to a higher number of electronic transitions and bandgap narrowing [38,59].

3.4 SEM Analysis

Pure CuO NPs (Fig. 6A) featured a heterogeneous distribution of particles with various morphologies, including uniform spherical NPs, flower-like structures, and hierarchical nanostructures. The high aggregation degree was ascribed to densification caused by the limited space between the particles. Higher-magnification analysis revealed a mixture of spherical and flower-like morphologies, with most NPs existing in an aggregated state [60]. The aver-

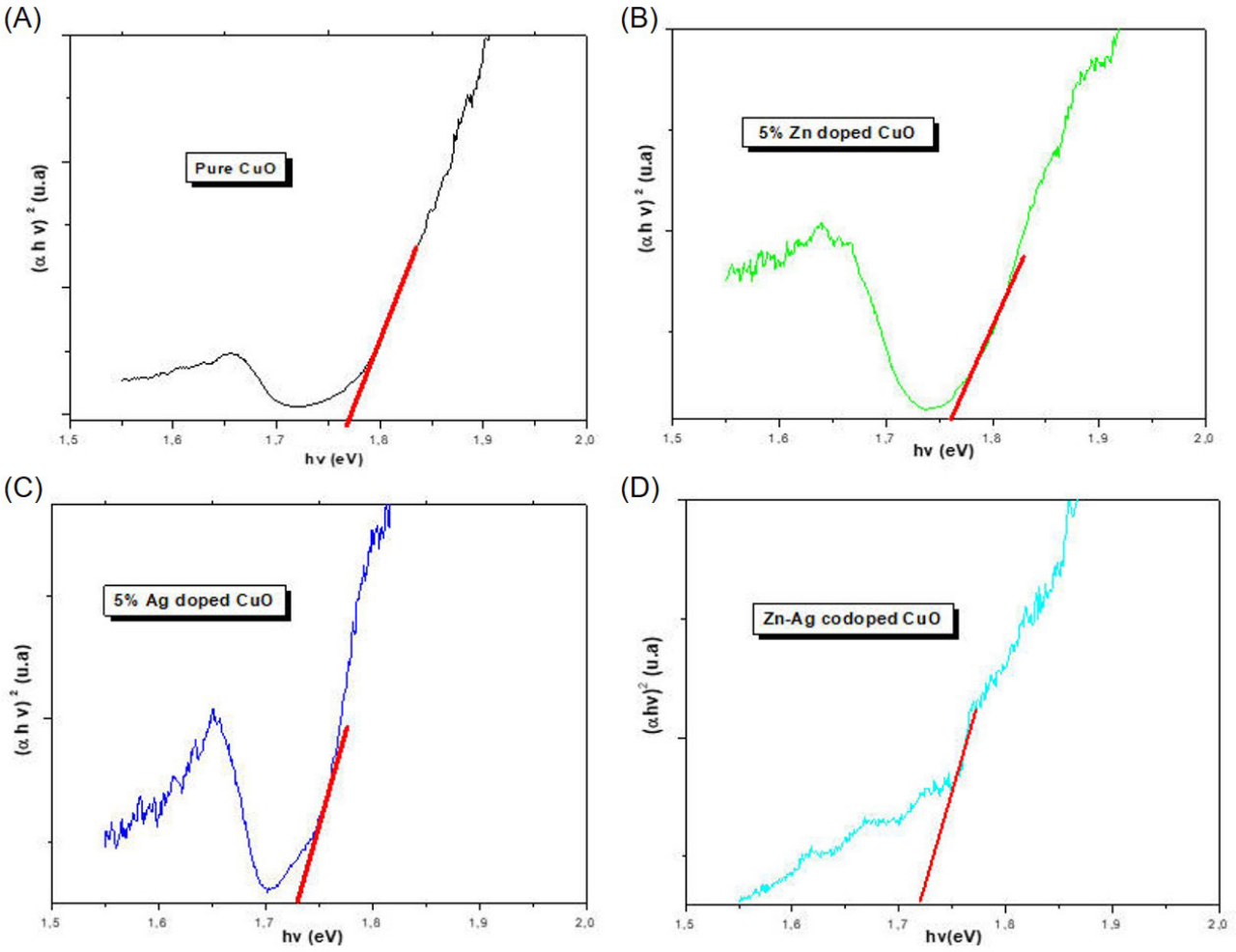

Fig. 5. Tauc plots used for bandgap determination. (A) pure CuO, (B) 5% Zn-doped CuO, (C) 5% Ag-doped CuO, (D) Zn-Ag codoped CuO.

age particle size was estimated as ~62 nm. Zn doping enhanced agglomeration (Fig. 6B). The particle size of Zn-doped NPs ranged from 216 to 331 nm, which aligns with previous findings [42]. Ag-doped CuO NPs (Fig. 6C) featured mixed nanostructures, including spherical pellet-like and disc-like ones [46]. The average size of the spherical NPs ranged from 192 to 228 nm. Ren et al. [61] reported a markedly smaller size range (20–25 nm) for spherical Ag-doped CuO NPs. Zn/Ag-codoped CuO NPs (Fig. 6D) featured a predominantly near-spherical morphology and porous nature and were notably less aggregated than pristine and single-metal-doped samples. The particle size and agglomeration behavior depended on the dopant: Zn doping increased particle size, while Ag doping had the opposite effect. This behavior was rationalized by considering the radii of Zn^{2+}, Ag^{+}, and Cu^{2+} [39]. The average size of the codoped sample ranged from 128 to 165 nm. A similar trend in crystallite size variation was also observed in the case of Zn/Ag-codoped CuO NPs [26]. However, the *D* values determined from XRD data (Table 1) are smaller than the sizes determined by SEM because the former reflect the sizes of single crystals, whereas the latter reflect the sizes of crystal aggregates. Similar trends have been widely reported for Ag/Co-codoped CuO [23].

Table 2. ZOI diameters of pure and doped CuO NPs.

NPs	ZOI diameter (mm) for *E. coli*	ZOI diameter (mm) for *S. aureus*
Pure CuO	17	4
Zn-doped CuO	18	20
Ag-doped CuO	19	17
Zn/Ag-codoped CuO	23	15

ZOI, zone-of-inhibition.

3.5 Antibacterial Activity

The antibacterial activities of pure and doped CuO NPs are illustrated in Fig. 7, with zone-of-inhibition (ZOI) diameters listed in Table 2. The activity of Zn-doped CuO NPs against *S. aureus* (ZOI diameter = 20 mm) exceeded that against *E. coli* (18 mm), in line with previous studies [62,63]. Conversely, the activity of Ag-doped CuO NPs

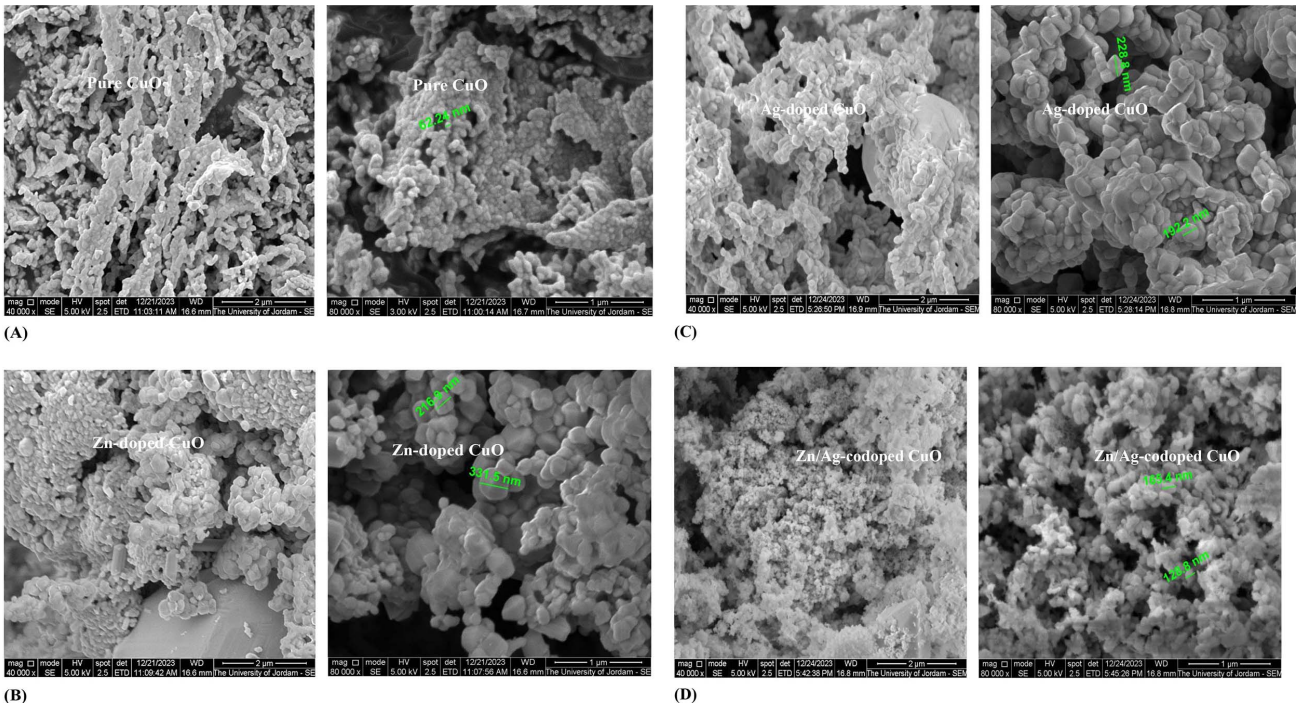

Fig. 6. SEM micrographs of (A) pure, (B) Zn-doped, (C) Ag-doped, and (D) Zn/Ag-codoped CuO NPs. Scale bar: 1 µm, 2 µm.

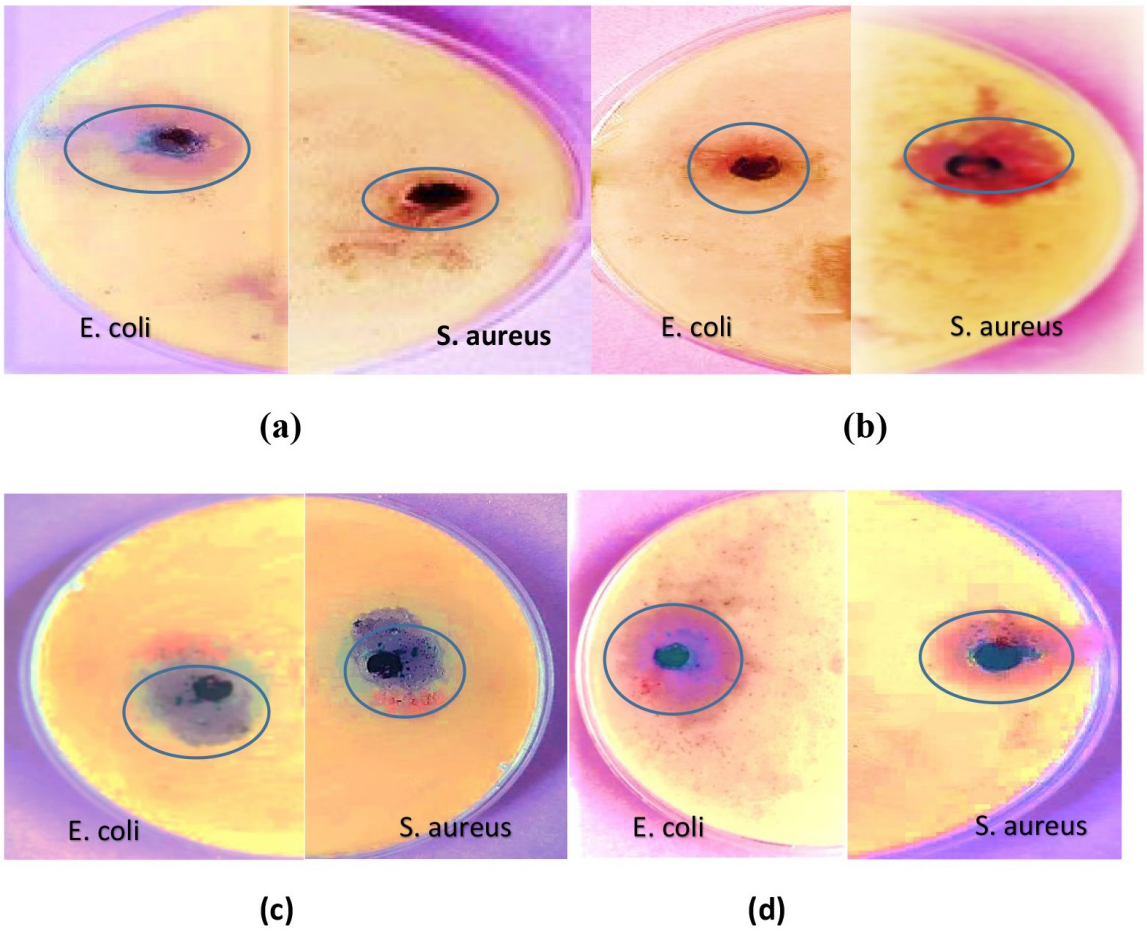

Fig. 7. Images illustrating the antibacterial activities of (a) pure, (b) Zn-doped, (c) Ag-doped, and (d) Zn-Agcodoped CuO NPs. Scale bar: 5 mm.

against *S. aureus* (17 mm) was lower than that against *E. coli* (19 mm), which contradicts the previously reported higher susceptibility of Gram-positive bacteria to antibacterial agents [64]. This discrepancy highlights the dependence of antibacterial properties on factors such as bacterial strain and dopant. The maximum ZOI diameter (23 mm) was observed for *E. coli* treated with Zn/Ag-codoped CuO NPs, revealing the selectivity of this material for Gram-negative bacteria.

The enhanced antibacterial activity of codoped CuO NPs was attributed to the production of ROS such as hydroxyl radicals, oxide radicals, and oxygen anion radicals. *E. coli* possesses a more negatively charged and rigid cell membrane than *S. aureus* [65]. The positively charged Zn and Ag centers in the codoped NPs might facilitate binding to the negatively charged bacterial cell walls and thus enhance the antibacterial effect. Additionally, codoping might promote the ability of CuO NPs to disrupt the bacterial cell membrane by creating pits and gaps [66,67].

This study demonstrates the potential for tailoring the antibacterial activity of CuO NPs through codoping with Zn and Ag. The observed selectivity for Gram-negative bacteria highlights the need for elucidating the underlying mechanisms.

3.6 Limitations

Despite the promising structural, optical, and antibacterial properties of pure and Zn–Ag co-doped CuO, this study has several limitations. The investigation was conducted under laboratory conditions using a limited number of pathogenic bacterial strains; therefore, the results may not fully represent the material's performance against a broader range of microorganisms or under real-world environmental conditions. In addition, the antibacterial mechanism was not investigated in detail, and further studies are required to clarify the respective contributions of metal-ion release, reactive oxygen species generation, and direct interaction between the nanoparticles and bacterial cells. The long-term stability, potential cytotoxicity, environmental impact, and biological safety of the prepared materials were also not evaluated. Finally, optimization of the Zn and Ag concentrations and assessment of the material's performance in practical applications are necessary before considering potential biomedical or environmental uses.

4. Conclusion

Pure and doped (Zn, Ag, or both) CuO NPs were synthesized and characterized in terms of physicochemical properties and activity against *E. coli* and *S. aureus*. All NPs featured a monoclinic tenorite structure, and doping enhanced crystallinity. Codoping with Zn and Ag led to the formation of additional phases, namely Zn–CuO and Ag–CuO. Crystallite size decreased upon doping, whereas dislocation density, strain, and unit cell volume increased. Sample morphology depended on dopant type, with structures ranging from spherical to flower-like and nanorod-like forms. Zn-doping increased particle size. In contrast, Ag doping produced the opposite effect, resulting in the formation of more uniformly distributed particles. The Zn/Ag-codoped sample displayed a near-spherical particle morphology. Codoping caused a red shift in the absorption edge and thus reduced the bandgap from 1.77 to 1.71 eV. Overall, this study shows that Zn/Ag codoping can be used to tailor the physicochemical and antibacterial properties of CuO NPs and thus render them suitable for medical and environmental applications requiring robust antibacterial activity.

Availability of Data and Materials

All data generated or analyzed during this study are included in this published article and its supplementary information files. The data supporting the findings of this study are available from the corresponding author upon reasonable request.

Author Contributions

AF and AS designed the research study. FH and ZA helped to perform the research. OA made substantial contributions to the conception and design of the work and to the acquisition, analysis, and interpretation of data, particularly regarding the antibacterial activity studies. OB helped analyze the data. AF wrote the manuscript. All authors contributed to editorial changes in the manuscript. All authors read and approved the final manuscript. All authors have participated sufficiently in the work and agreed to be accountable for all aspects of the work.

Ethics Approval and Consent to Participate

Not applicable.

Acknowledgment

We would like to express our gratitude to all those who helped us during the writing of this manuscript. Thanks to all the peer reviewers for their opinions and suggestions.

Funding

This research received no external funding.

Conflicts of Interest

The authors declare no conflicts of interest.

References

[1] Hou X, Zaks T, Langer R, Dong Y. Lipid nanoparticles for mRNA delivery. Nature Reviews Materials. 2021; 6: 1078–1094. https://doi.org/10.1038/s41578-021-00358-0

[2] Lim SH, Yee GT, Khang D. Nanoparticle-Based Combinational Strategies for Overcoming the Blood-Brain Barrier and Blood-Tumor Barrier. International Journal of Nanomedicine. 2024; 19: 2529–2552. https://doi.org/10.2147/IJN.S450853

[3] Singh R, Lillard JW. Nanoparticle-based targeted drug delivery.

Experimental and Molecular Pathology. 2009; 86: 215–223. https://doi.org/10.1016/j.yexmp.2008.12.004
[4] Negrescu AM, Killian MS, Raghu SNV, Schmuki P, Mazare A, Cimpean A. Metal Oxide Nanoparticles: Review of Synthesis, Characterization and Biological Effects. Journal of Functional Biomaterials. 2022; 13: 274. https://doi.org/10.3390/jfb13040274
[5] Maraj M, Raza A, Wang X, Chen J, Riaz KN, Sun W. Mo-doped CuO nanomaterial for photocatalytic degradation of water pollutants under visible light. Catalysts. 2021; 11: 1198. https://doi.org/10.3390/catal11101198
[6] Sun L, Zhuang Y, Yuan Y, Zhan W, Wang XJ, Han X, et al. Nitrogen-doped carbon-coated CuO-In2O3 p-n heterojunction for remarkable photocatalytic hydrogen evolution. Advanced Energy Materials. 2019; 9: 1902839. https://doi.org/10.1002/aenm.201902839
[7] Johan MR, Suan MS, Hawari NL, Ching HA. Annealing effects on the properties of copper oxide thin films prepared by chemical deposition. International Journal of Electrochemical Science. 2011; 6: 6094–6104. https://doi.org/10.1016/S1452-3981(23)19665-9
[8] Kose S, Atay FE, Bilgin Vİ, Akyuz I. Some physical properties of copper oxide films: the effect of substrate temperature. Materials Chemistry and Physics. 2008; 111: 351–358. https://doi.org/10.1016/j.matchemphys.2008.04.025
[9] Motshekga SC. Structural and antibacterial properties of copper oxide nanoparticles: a study on the effect of calcination temperature. Nano Express. 2024; 5: 015011. https://doi.org/10.1088/2632-959X/ad228d
[10] Zhang L, Gao Z, Liu C, Ren L, Tu Z, Liu R, et al. N-doped nanoporous graphene decorated three-dimensional CuO nanowire network and its application to photocatalytic degradation of dyes. RSC advances. 2014; 4: 47455–47460. https://doi.org/10.1039/c4ra06872f
[11] Ruvalcaba-Ontiveros RI, Esparza-Ponce HE, Reyes-Martínez R, Manjarrez-Nevárez LA, Gómez-Benítez V, Piñon-Castillo HA. Antibacterial Activity of CuO Nanoparticles, Ethanolic Extract of Amphipterygium adstringens, and Their Combination Against Multidrug-Resistant Bacteria. International Journal of Nanomedicine. 2025; 20: 8003–8022. https://doi.org/10.2147/IJN.S517465
[12] Gudkov SV, Burmistrov DE, Fomina PA, Validov SZ, Kozlov VA. Antibacterial Properties of Copper Oxide Nanoparticles (Review). International Journal of Molecular Sciences. 2024; 25: 11563. https://doi.org/10.3390/ijms252111563
[13] Fterich M, Nasr FB, Lefi R, Toumi M, Guermazi S. Effect of concentration of hexamethylenetetramine in structure, microstructure and optical properties of CuO nanoparticles synthesized by hydrothermal route. Materials Science in Semiconductor Processing. 2016; 43: 114–122. https://doi.org/10.1016/j.mssp.2015.11.023
[14] Singh J, Sharma S, Soni S, Sharma S, Singh RC. Influence of different milling media on structural, morphological and optical properties of the ZnO nanoparticles synthesized by ball milling process. Materials Science in Semiconductor Processing. 2019; 98: 29–38. https://doi.org/10.1016/j.mssp.2019.03.026
[15] Attou L, Jaber B, Ez-Zahraouy H. Effect of annealing temperature on structural, optical and photocatalytic properties of CuO nanoparticles. Mediterranean Journal of Chemistry. 2018; 7: 308–316.
[16] Heinemann M, Eifert B, Heiliger C. Band structure and phase stability of the copper oxides Cu2O, CuO, and Cu4O3. Physical Review B—Condensed Matter and Materials Physics. 2013; 87: 115111. https://doi.org/10.1103/PhysRevB.87.115111
[17] Vinothkanna A, Mathivanan K, Ananth S, Ma Y, Sekar S. Biosynthesis of copper oxide nanoparticles using Rubia cordifolia bark extract: characterization, antibacterial, antioxidant, larvicidal and photocatalytic activities. Environmental Science and Pollution Research International. 2023; 30: 42563–42574. https://doi.org/10.1007/s11356-022-18996-4
[18] Sethuraman RG, Venkatachalam T, Kirupha SD. Fabrication and characterization of Zn doped CuO nanofiber using newly designed nanofiber generator for the photodegradation of methylene blue from textile effluent. Materials Science-Poland. 2018; 36: 520–529. https://doi.org/10.2478/msp-2018-0056
[19] Viruthagiri G, Gopinathan E, Shanmugam N, Gobi R. Synthesis and characterization of ZrO2-CuO co-doped ceria nanoparticles via chemical precipitation method. Spectrochimica Acta. Part A, Molecular and Biomolecular Spectroscopy. 2014; 131: 556–563. https://doi.org/10.1016/j.saa.2014.04.117
[20] Basith NM, Vijaya JJ, Kennedy LJ, Bououdina M. Structural, morphological, optical, and magnetic properties of Ni-doped CuO nanostructures prepared by a rapid microwave combustion method. Materials Science in Semiconductor Processing. 2014; 17: 110–118. https://doi.org/10.1016/j.mssp.2013.09.013
[21] Yadav V, Shukla R, Sharma KS, Ohjha S. Study of Structural and Optical Properties of Copper, Manganese, and Mixed Metal (Cu And Mn) Oxide Nanoparticles. Current Nanomaterials. 2025; 10: 78–85. https://doi.org/10.2174/2405461508666230627144618
[22] Bayansal F, Taşköprü T, Şahin B, Çetinkara HA. Effect of cobalt doping on nanostructured CuO thin films. Metallurgical and Materials Transactions A. 2014; 45: 3670–3674. https://doi.org/10.1007/s11661-014-2306-1
[23] Thakur N, Kumar K. Effect of (Ag, Co) co-doping on the structural and antibacterial efficiency of CuO nanoparticles: A rapid microwave assisted method. Journal of Environmental Chemical Engineering. 2020; 8: 104011. https://doi.org/10.1016/j.jece.2020.104011
[24] El Sayed AM, Shaban M. Structural, optical and photocatalytic properties of Fe and (Co, Fe) co-doped copper oxide spin coated films. Spectrochimica Acta. Part A, Molecular and Biomolecular Spectroscopy. 2015; 149: 638–646. https://doi.org/10.1016/j.saa.2015.05.010
[25] Anu, Thakur N, Kumar K, Sharma KK. Application of Co-doped copper oxide nanoparticles against different multidrug resistance bacteria. Inorganic and Nano-Metal Chemistry. 2020; 50: 933–943. https://doi.org/10.1080/24701556.2020.1728554
[26] Thakur N, Anu, Kumar K, Kumar A. Effect of (Ag, Zn) co-doping on structural, optical and bactericidal properties of CuO nanoparticles synthesized by a microwave-assisted method. Dalton Transactions (Cambridge, England: 2003). 2021; 50: 6188–6203. https://doi.org/10.1039/d0dt04405a
[27] Hans M, Erbe A, Mathews S, Chen Y, Solioz M, Mücklich F. Role of copper oxides in contact killing of bacteria. Langmuir: the ACS Journal of Surfaces and Colloids. 2013; 29: 16160–16166. https://doi.org/10.1021/la404091z
[28] Zhang L, Jiang Y, Ding Y, Povey M, York D. Investigation into the antibacterial behaviour of suspensions of ZnO nanoparticles (ZnO nanofluids). Journal of Nanoparticle Research. 2007; 9: 479–489. https://doi.org/10.1007/s11051-006-9150-1
[29] Applerot G, Lipovsky A, Dror R, Perkas N, Nitzan Y, Lubart R, et al. Enhanced antibacterial activity of nanocrystalline ZnO due to increased ROS-mediated cell injury. Advanced Functional Materials. 2009; 19: 842–852. https://doi.org/10.1002/adfm.200801081
[30] Malka E, Perelshtein I, Lipovsky A, Shalom Y, Naparstek L, Perkas N, et al. Eradication of multi-drug resistant bacteria by a novel Zn-doped CuO nanocomposite. Small (Weinheim an Der Bergstrasse, Germany). 2013; 9: 4069–4076. https://doi.org/10.1002/smll.201301081
[31] Prabhakaran D, Boothroyd AT. Single crystal growth of

Zn-doped CuO by the floating-zone method. Journal of Crystal Growth. 2003; 250: 77–82. https://doi.org/10.1016/S0022-0248(02)02230-3
[32] Azam A, Ahmed AS, Oves M, Khan MS, Memic A. Size-dependent antimicrobial properties of CuO nanoparticles against Gram-positive and -negative bacterial strains. International Journal of Nanomedicine. 2012; 7: 3527–3535. https://doi.org/10.2147/IJN.S29020
[33] Dadi R, Azouani R, Traore M, Mielcarek C, Kanaev A. Antibacterial activity of ZnO and CuO nanoparticles against gram positive and gram negative strains. Materials Science & Engineering. C, Materials for Biological Applications. 2019; 104: 109968. https://doi.org/10.1016/j.msec.2019.109968
[34] Habeeb SA, Hammadi AH, Salman HD, Abed DA. Synthesis, characterization and antibacterial activities of Ag/CuO nanocomposites. Oxford Open Materials Science. 2025; 5: itaf014. https://doi.org/10.1093/oxfmat/itaf014
[35] Eshed M, Lellouche J, Gedanken A, Banin E. A Zn-Doped CuO Nanocomposite Shows Enhanced Antibiofilm and Antibacterial Activities Against Streptococcus Mutans Compared to Nano-sized CuO. Advanced Functional Materials. 2014; 24: 1382–1390. https://doi.org/10.1002/adfm.201302425
[36] Wu R, Zhang H, Pan J, Zhu H, Ma Y, Cui W, et al. Spatio-Design of Multidimensional Prickly Zn-Doped CuO Nanoparticle for Efficient Bacterial Killing. Advanced Materials Interfaces. 2016; 3: 1600472. https://doi.org/10.1002/admi.201600472
[37] Sharma S, Kumar K. Aloe-vera leaf extract as a green agent for the synthesis of CuO nanoparticles inactivating bacterial pathogens and dye. Journal of Dispersion Science and Technology. 2021; 42: 1950–1962. https://doi.org/10.1080/01932691.2020.1791719
[38] D M, Peddi KM, R R. CuO NANOPARTICLES: SYNTHESIS, CHARACTERIZATION AND THEIR BACTERICIDAL EFFICACY. International Journal of Applied Pharmaceutics. 2017; 9: 71–74. https://doi.org/10.22159/ijap.2017v9i6.71757
[39] Asamoah RB, Annan E, Mensah B, Nbelayim P, Apalangya V, Onwona-Agyeman B, et al. A comparative study of antibacterial activity of CuO/Ag and ZnO/Ag nanocomposites. Advances in Materials Science and Engineering. 2020; 2020: 7814324. https://doi.org/10.1155/2020/7814324
[40] Huang C, Tian X, Liu J, Wang W, Dong Z, Liu L. Fabrication of a single CuO nanowire-based gas sensor working at room temperature. 2013 International Conference on Manipulation, Manufacturing and Measurement on the Nanoscale (pp. 108–113). Suzhou, China. IEEE. 2013. https://doi.org/10.1109/3M-NANO.2013.6737394
[41] Lu J, Wang H, Dong S, Wang F, Dong Y. Effect of Ag shapes and surface compositions on the photocatalytic performance of Ag/ZnO nanorods. Journal of Alloys and Compounds. 2014; 617: 869–876. https://doi.org/10.1016/j.jallcom.2014.08.096
[42] Das S, Alford TL. Structural and optical properties of Ag-doped copper oxide thin films on polyethylene napthalate substrate prepared by low temperature microwave annealing. Journal of Applied Physics. 2013; 113: 244905. https://doi.org/10.1063/1.4812584
[43] Vikal S, Gautam YK, Kumar A, Kumar A, Singh N, Singh H, et al. Effect of silver (Ag) doping on structural, optical and antimicrobial properties of copper oxide (CuO) nanostructures. Nano Express. 2023; 4: 025004. https://doi.org/10.1088/2632-959X/acdc41
[44] Benrezgua E, Deghfel B, Zoukel A, Basirun WJ, Amari R, Boukhari A, et al. Synthesis and properties of copper doped zinc oxide thin films by sol-gel, spin coating and dipping: A characterization review. Journal of Molecular Structure. 2022; 1267: 133639. https://doi.org/10.1016/j.molstruc.2022.133639
[45] Nesa M, Sharmin M, Hossain KS, Bhuiyan AH. Structural, morphological, optical and electrical properties of spray deposited zinc doped copper oxide thin films. Journal of Materials Science: Materials in Electronics. 2017; 28: 12523–12534. https://doi.org/10.1007/s10854-017-7075-3
[46] Menazea AA, Mostafa AM. Ag doped CuO thin film prepared via pulsed laser deposition for 4-nitrophenol degradation. Journal of Environmental Chemical Engineering. 2020; 8: 104104. https://doi.org/10.1016/j.jece.2020.104104
[47] Kadam LD, Patil PS. Thickness-dependent properties of sprayed cobalt oxide thin films. Materials Chemistry and Physics. 2001; 68: 225–232. https://doi.org/10.1016/S0254-0584(00)00367-9
[48] Sebastian T, Jayakrishnan R, Kartha CS, Vijayakumar KP. Characterization of spray pyrolysed CuInS2 thin films. The Open Surface Science Journal. 2009; 1: 1–6. https://doi.org/10.2174/1876531900901010001
[49] Khmissi H, El Sayed AM, Shaban M. Structural, morphological, optical properties and wettability of spin-coated copper oxide; influences of film thickness, Ni, and (La, Ni) co-doping. Journal of Materials Science. 2016; 51: 5924–5938. https://doi.org/10.1007/s10853-016-9894-7
[50] Anand GT, Sundaram SJ, Kanimozhi K, Nithiyavathi R, Kaviyarasu K. Microwave assisted green synthesis of CuO nanoparticles for environmental applications. Materials Today: Proceedings. 2021; 36: 427–434. https://doi.org/10.1016/j.matpr.2020.04.881
[51] Alghamdi HA. Structural, morphological, optical, and electrical characteristics of polyethylene oxide/chitosan-copper oxide nanoparticles for optoelectronic applications. Optical Materials. 2022; 134: 113101. https://doi.org/10.1016/j.optmat.2022.113101
[52] Chen ZY, Shao WZ, Li WJ, Sun XY, Zhen L, Li Y. Tuning the interface adhesion of Ag/ZnO composites by metallic dopants: A DFT study. Computational Materials Science. 2023; 224: 112151. https://doi.org/10.1016/j.commatsci.2023.112151
[53] Méndez-Medrano MG, Kowalska E, Lehoux A, Herissan A, Ohtani B, Bahena D, et al. Surface modification of TiO2 with Ag nanoparticles and CuO nanoclusters for application in photocatalysis. The Journal of Physical Chemistry C. 2016; 120: 5143–5154. https://doi.org/10.1021/acs.jpcc.5b10703
[54] Mukherjee N, Show B, Maji SK, Madhu U, Bhar SK, Mitra BC, et al. CuO nano-whiskers: electrodeposition, Raman analysis, photoluminescence study and photocatalytic activity. Materials Letters. 2011; 65: 3248–3250. https://doi.org/10.1016/j.matlet.2011.07.016
[55] Bhuvaneshwari S, Gopalakrishnan N. Hydrothermally synthesized Copper Oxide (CuO) superstructures for ammonia sensing. Journal of Colloid and Interface Science. 2016; 480: 76–84. https://doi.org/10.1016/j.jcis.2016.07.004
[56] Wang Y, Jiang T, Meng D, Kong J, Jia H, Yu M. Controllable fabrication of nanostructured copper compound on a Cu substrate by a one-step route. RSC Advances. 2015; 5: 16277–16283. https://doi.org/10.1039/c4ra14523b
[57] Wang Y, Cao L, Li J, Kou L, Huang J, Feng Y, et al. Cu/Cu2O@Ppy nanowires as a long-life and high-capacity anode for lithium ion battery. Chemical Engineering Journal. 2020; 391: 123597. https://doi.org/10.1016/j.cej.2019.123597
[58] Tauc J. Optical properties and electronic structure of amorphous semiconductors. In Nudelman S, Mitra SS (eds.) Optical Properties of Solids (pp. 123–136). Springer: Boston, MA. 1969. https://doi.org/10.1007/978-1-4757-1123-3_5
[59] Wang F, Guo Z. Facile fabrication of ultraviolet light cured fluorinated polymer layer for smart superhydrophobic surface with excellent durability and flame retardancy. Journal of Colloid and Interface Science. 2019; 547: 153–161. https://doi.org/10.1016/j.jcis.2019.03.095
[60] Wang J, He S, Li Z, Jing X, Zhang M, Jiang Z. Self-assembled

CuO nanoarchitectures and their catalytic activity in the thermal decomposition of ammonium perchlorate. Colloid and Polymer Science. 2009; 287: 853–858. https://doi.org/10.1007/s00396-009-2040-1

[61] Ren C, Yang B, Wu M, Xu J, Fu Z, Lv Y, et al. Synthesis of Ag/ZnO nanorods array with enhanced photocatalytic performance. Journal of Hazardous Materials. 2010; 182: 123–129. https://doi.org/10.1016/j.jhazmat.2010.05.141

[62] Sharma S, Kumar K, Thakur N, Chauhan S, Chauhan MS. The effect of shape and size of ZnO nanoparticles on their antimicrobial and photocatalytic activities: a green approach. Bulletin of Materials Science. 2020; 43: 20. https://doi.org/10.1007/s12034-019-1986-y

[63] Sharma S, Kumar K, Thakur N, Chauhan MS. Ocimum tenuiflorum leaf extract as a green mediator for the synthesis of ZnO nanocapsules inactivating bacterial pathogens. Chemical Papers. 2020; 74: 3431–3444. https://doi.org/10.1007/s11696-020-01177-3

[64] Jatoi AW, Ogasawara H, Kim IS, Ni QQ. Cellulose acetate/multi-wall carbon nanotube/Ag nanofiber composite for antibacterial applications. Materials Science & Engineering. C, Materials for Biological Applications. 2020; 110: 110679. https://doi.org/10.1016/j.msec.2020.110679

[65] Anitha S, Muthukumaran S. Structural, optical and antibacterial investigation of La, Cu dual doped ZnO nanoparticles prepared by co-precipitation method. Materials Science & Engineering. C, Materials for Biological Applications. 2020; 108: 110387. https://doi.org/10.1016/j.msec.2019.110387

[66] Khatoon UT, Velidandi A, Rao GN. Copper oxide nanoparticles: synthesis via chemical reduction, characterization, antibacterial activity, and possible mechanism involved. Inorganic Chemistry Communications. 2023; 149: 110372. https://doi.org/10.1016/j.inoche.2022.110372

[67] Sharma S, Kumar K, Thakur N. Green synthesis of silver nanoparticles and evaluation of their anti-bacterial activities: use of Aloe barbadensis miller and Ocimum tenuiflorum leaf extracts. Nanofabrication. 2021; 6: 52–67. https://doi.org/10.1515/nanofab-2020-0102